CORE

Metadata, citation and similar papers at core.ac.uk

Provided by Radboud Repository

Radboud Repository

Radboud University Nijmegen

PDF hosted at the Radboud Repository of the Radboud University Nijmegen

The following full text is a publisher's version.

For additional information about this publication click this link.
http://hdl.handle.net/2066/206118

Please be advised that this information was generated on 2020-01-01 and may be subject to change.

SCIENCE ADVANCES | RESEARCH ARTICLE

CHEMISTRY

Copyright © 2019
The Authors, some
rights reserved;
exclusive licensee
American Association
for the Advancement
of Science. No claim to
original U.S. Government
Works. Distributed
under a Creative
Commons Attribution
NonCommercial
License 4.0 (CC BY-NC).

Acid solvation versus dissociation at "stardust conditions": Reaction sequence matters

Devendra Mani[1], Ricardo Pérez de Tudela[2], Raffael Schwan[1], Nitish Pal[1], Saskia Körning[2], Harald Forbert[2], Britta Redlich[3], A. F. G. van der Meer[3], Gerhard Schwaab[1], Dominik Marx[2]*, Martina Havenith[1]*

Chemical reactions at ultralow temperatures are of fundamental importance to primordial molecular evolution as it occurs on icy mantles of dust nanoparticles or on ultracold water clusters in dense interstellar clouds. As we show, studying reactions in a stepwise manner in ultracold helium nanodroplets by mass-selective infrared (IR) spectroscopy provides an avenue to mimic these "stardust conditions" in the laboratory. In our joint experimental/theoretical study, in which we successively add H_2O molecules to HCl, we disclose a unique IR fingerprint at 1337 cm^{-1} that heralds hydronium (H_3O^+) formation and, thus, acid dissociation generating solvated protons. In stark contrast, no reaction is observed when reversing the sequence by allowing HCl to interact with preformed small embryonic ice-like clusters. Our ab initio simulations demonstrate that not only reaction stoichiometry but also the reaction sequence needs to be explicitly considered to rationalize ultracold chemistry.

INTRODUCTION

Acid dissociation, proton solvation, and charge defect migration in aqueous environments all play a fundamental role in a plethora of processes ranging from chemistry and physics to biology and, therefore, have been analyzed in utmost molecular detail using infrared (IR) spectroscopy in both the gas and condensed phases (*1*–*15*). While thermal fluctuations and vivid H-bond dynamics are pivotal at ambient conditions (*16*), distinctly different mechanisms take over at lower temperatures, for instance, enabling HCl-induced acid/base chemistry on ice grains in Earth's stratospheric clouds (*2*, *17*–*19*). Water ices are also abundant in the solar system and are found in interstellar space (*20*–*22*), and they are probable candidates for the source of water on planets including Earth (*23*, *24*).

In dense interstellar clouds, much lower temperatures of the order of only 10 K or even less govern the chemistry on icy dust grains (*22*, *25*). A fundamental question is whether acid/base chemistry, such as discovered in stratospheric clouds, could already be triggered at these ultracold "stardust conditions" by dissociation of acids, e.g., HCl, in the absence of thermal and photoinduced activation. This is highly relevant to early chemical evolution, long before more complex prebiotic chemistry came on the scene.

HCl uptake on ice crystals in polar stratospheric clouds (PSCs) catalyzes the formation of molecular chlorine (Cl_2) (*26*, *27*). Most of the experimental studies confirm that at PSC temperatures (about 190 K), the ionized form of HCl prevails on ice surfaces (*2*, *28*–*31*). However, the results at lower temperatures remain ambiguous. Kang *et al.* (*28*), using Cs^+ reactive ion scattering and secondary ion mass spectrometry, and Devlin *et al.* (*2*), using Fourier transform IR spectroscopic techniques, proposed that no ionization takes place below 50 K, whereas on increasing temperature, the rate of ionization was found to increase: from ~15% at 60 K to almost complete ionization taking place at 90 to 95 K. In contrast, Parent and Laffon (*29*) reported an ionization rate of 80% even at temperatures of 20 K. In a succeeding study (*31*), 92% ionization of HCl was reported at 50 K. These ionization rates were found to be independent of temperature, as they were similar for 50 and 90 K, supporting the theoretical prediction that HCl dissociation on ice surfaces is a barrierless process (*19*). These results gave rise to a controversial discussion on the rate of HCl ionization on ice surfaces (*32*, *33*).

Here, we report the results of a joint experimental/theoretical study of the generic HCl-water system in superfluid helium nanodroplets, which are known to enable the controlled formation of H-bonded molecular aggregates at ultracold conditions of 0.37 K (*34*). Using the high-intensity pulsed free-electron lasers (FELs) at FELIX in Nijmegen, our measurements were performed in the IR fingerprint region (about 1000 to 1700 cm^{-1}) based on the recently developed BoHeNDI@FELIX end station (*35*).

In our efforts of establishing a nanolab for molecularly controlled cryochemical synthesis, the pickup chamber of BoHeNDI@FELIX hosts two distinct pickup cells—denoted as cell 1 and cell 2 in the following—each of them with a 5-mm orifice (where cross-contamination from one cell to the other is restricted by low background pressure together with their large separation, 20 cm; see fig. S1). This end station enables us to control the sequence and the pressure for each dopant independently, i.e., we can now choose whether we seed the nanodroplets with HCl in the first cell followed by subsequent pickup of water in the second cell or vice versa. The ultrabright FELs at FELIX (up to 80-mJ energy per 5- to 8-μs duration pulse) allow us to record mass-selective IR spectra with a good signal-to-noise (S/N) ratio. FELIX also allows access to the important IR fingerprint region for acid formation, which is crucial for unambiguous detection of acid formation.

Upon sequential microsolvation of HCl by H_2O molecules, we earlier discovered a peculiar reaction mechanism—aggregation-induced dissociation—which allows acid dissociation even at 0.37 K (*9*, *10*, *36*). According to this mechanism, the dissociation reaction producing hydronium, H_3O^+, proceeds by bypassing deep potential energy minima, which would be impossible to surmount at ultracold conditions (*34*). Adding the fourth water molecule yields the solvent-shared ion pair (SIP), $H_3O^+(H_2O)_3Cl^-$ [see molecular models in Fig. 1 (B and C)], as depicted in the left reaction channel of Fig. 2.

---

[1]Lehrstuhl für Physikalische Chemie II, Ruhr-Universität Bochum, 44801 Bochum, Germany. [2]Lehrstuhl für Theoretische Chemie, Ruhr-Universität Bochum, 44780 Bochum, Germany. [3]FELIX Laboratory, Institute for Molecules and Materials, Radboud University, 6325 ED Nijmegen, Netherlands.
*Corresponding author. Email: martina.havenith@rub.de (M.H.); dominik.marx@rub.de (D.M.)

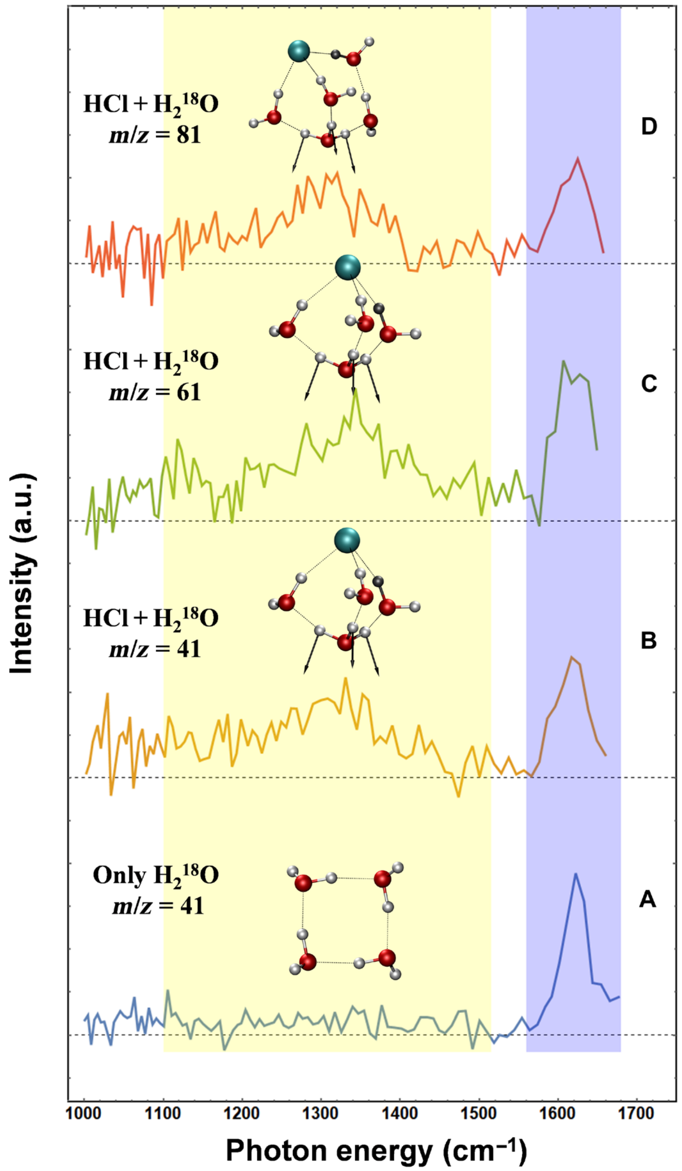

Fig. 1. IR depletion spectra of pure water and mixed HCl-water clusters, resulting from pickup sequence cell 1 (HCl) and cell 2 (water), measured at different mass channels. (**A**) IR spectra of pure $H_2{}^{18}O$ clusters, measured at $m/z = 41$. (**B** to **D**) Spectra in the presence of a small amount of HCl gas, measured at $m/z = 41$, 61, and 81, respectively. These mass channels correspond to $H^+(H_2{}^{18}O)_2$ ($m/z = 41$), $H^+(H_2{}^{18}O)_3$ ($m/z = 61$), and $H^+(H_2{}^{18}O)_4$ ($m/z = 81$) fragments. The bands corresponding to the bending vibration of the pure water $(H_2O)_n$ ($n = 4$ and 5) clusters are highlighted in the light blue shade. The broad band highlighted in yellow is assigned to the umbrella mode of the H_3O^+ core of the dissociated species. HCl partial pressure of 0.14 mPa and water partial pressure of 0.53 mPa were used in all the measurements. The proton originating from HCl is shown in dark gray. a.u., arbitrary units.

The alternative synthesis pathway involves aggregation of a specific number of H_2O molecules as the first step, followed by a pickup of one HCl molecule. At the ultralow temperatures in helium nanodroplets, water molecules aggregate into cyclic H-bonded structures, leading eventually to the "smallest piece of ice" (*34*). But what is the fate of an acid molecule if attached to these ice-like complexes? Knowing that four H_2O molecules suffice to dissociate HCl in helium nanodroplets (*9*, *10*), the interesting question is how, or even if, the acid can dissociate and transfer its proton to these preexisting embryonic ice-like structures at ultracold conditions.

RESULTS AND DISCUSSION

To unambiguously unravel the chemistry resulting from the two pickup sequences, we used isotopically pure $H_2{}^{18}O$. Whereas $H^+(H^{35}Cl)_n$ and $H^+(H_2{}^{16}O)_{2n}$ ionization fragments are detected at the same [mass/charge ratio (m/z)] channel in the mass spectrometer, these fragments can be separated in the case of $H^+(H^{35}Cl)_n$ and $H^+(H_2{}^{18}O)_{2n}$ [see also (*10*)]. We recorded the IR spectrum of pure $H_2{}^{18}O$ clusters (cell 2, 0.53 mPa $H_2{}^{18}O$) at $m/z = 41$ [which corresponds to the $H^+(H_2{}^{18}O)_2$ fragment]. Because molecular pickup by helium droplets follows Poisson statistics (*37*), at this partial pressure of water, the relative size distribution of water clusters could be estimated to be tetramer (~55%), pentamer (~30%), and hexamer (~15%). The well-known fingerprint of the water bend was observed around 1620 cm^{-1}, which arises predominantly from $(H_2{}^{18}O)_4$ (see Fig. 1A) (*38*). When adding HCl in the first cell and $H_2{}^{18}O$ in the second cell in our cryo-nanolab (cell 1, 0.14 mPa HCl; cell 2, 0.53 mPa $H_2{}^{18}O$), we observed a broad absorption band centered at ~1337 cm^{-1} (see Fig. 1B), in agreement with the theoretical predictions for the unique spectroscopic fingerprint of the (hindered) umbrella motion of H_3O^+ at 1357 cm^{-1} (*39*). This is characteristic of the SIP conformer of the "smallest droplet of dissociated HCl acid" (*9*, *10*, *36*). At these experimental conditions, 0.5 HCl and three water molecules are picked up on average, yielding a preference for clusters doped with a single HCl and a distribution of water cluster sizes ranging from $n = 2$ to 5. The mass-selective depletion pickup curves (see fig. S5) reveal that the spectroscopic signal at 1320 cm^{-1} (see Fig. 1B) is dominated by a cluster with one HCl and four water molecules, as expected for the smallest droplet of acid. The fingerprint region, as reported here, has the advantage that the hydronium umbrella motion (*39*) of the smallest droplet of acid is uncongested, in contrast to the higher frequency range (2100 to 2900 cm^{-1}) where the modes are strongly coupled and the spectroscopic signatures for dissociation overlap with the bands from undissociated $(HCl)_m(H_2O)_n$ clusters, which, in the past, led to a controversial discussion about the experimental verification of HCl dissociation for a cluster with one HCl and four water molecules (*9*, *10*, *40*).

Having shown that four water molecules are sufficient to dissociate HCl, we investigated whether larger dissociated clusters contribute to the observed spectroscopic signal. Spectra recorded at $m/z = 61$ [$H^+(H_2{}^{18}O)_3$ fragment] and $m/z = 81$ [$H^+(H_2{}^{18}O)_4$ fragment] are depicted in Fig. 1, C and D, respectively. The pressure variance of the band intensity reveals that the band at $m/z = 61$ is dominated by clusters containing four water molecules, whereas the band at $m/z = 81$ and 1250 cm^{-1} shows contributions from dissociated clusters containing five (or more) water molecules (Table 1; see the "The umbrella motion of hydronium: Parent cluster size determination" section in the Supplementary Materials for more details). The hydronium band is red-shifted when recorded at $m/z = 81$ compared to the band recorded at $m/z = 61$.

In an effort to characterize the formed ion pair species containing five water molecules (Fig. 1D), ab initio aggregation simulations (*36*) were performed to disclose what happens if the fifth water molecule reacts with SIP (see the "Ab initio aggregation simulations of SIP with the fifth H_2O molecule" section in the Supplementary Materials). They unveil that only two specific ion pair structures out of many

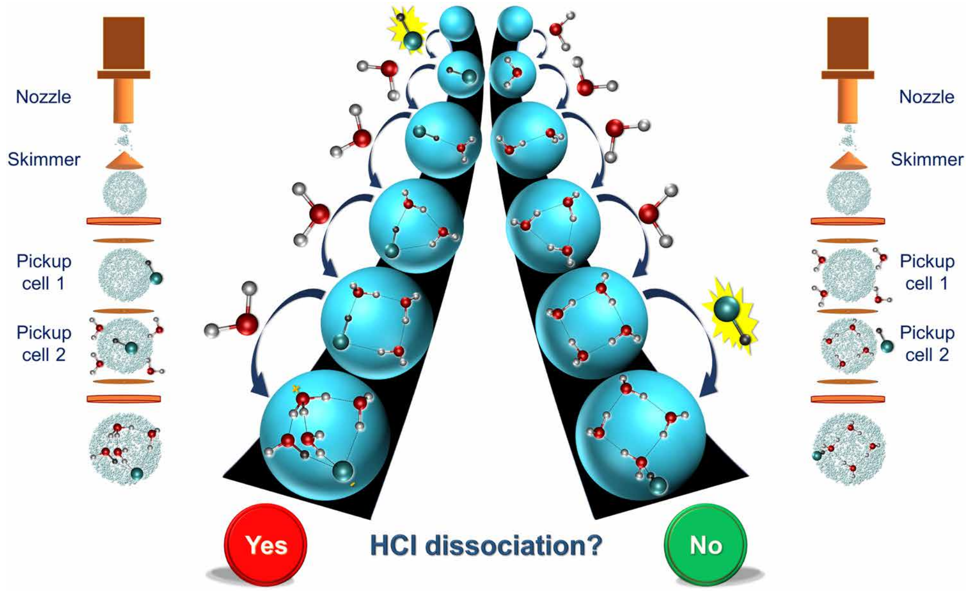

Fig. 2. Two different pathways for the aggregation of $HCl(H_2O)_4$ clusters in helium droplets, depicting that acid formation at ultracold temperatures follows a unique pathway. (**Left**) The first HCl and, subsequently, four water molecules are picked up, yielding aggregation-induced dissociation of HCl and the formation of the smallest droplet of acid, $H_3O^+(H_2O)_3Cl^-$. (**Right**) The first four water molecules aggregate to form a cyclic water tetramer, and upon subsequent addition of one HCl molecule, the HCl is found to remain undissociated.

Table 1. Number of water molecules (*n*) contributing to the observed bands, determined from the fit of the pressure-dependent spectroscopic signal to Poisson distributions. The pickup curves were recorded at a particular on-resonance frequency. See also the "Ionization mechanism of pure water and mixed HCl-water aggregates" and "The umbrella motion of hydronium: Parent cluster size determination" sections in the Supplementary Materials.

Resonance frequency (cm^{-1})	Mass channel (atomic mass units)	*n*
1320	41	4
1320	61	4
1400	61	4
1250	81	5

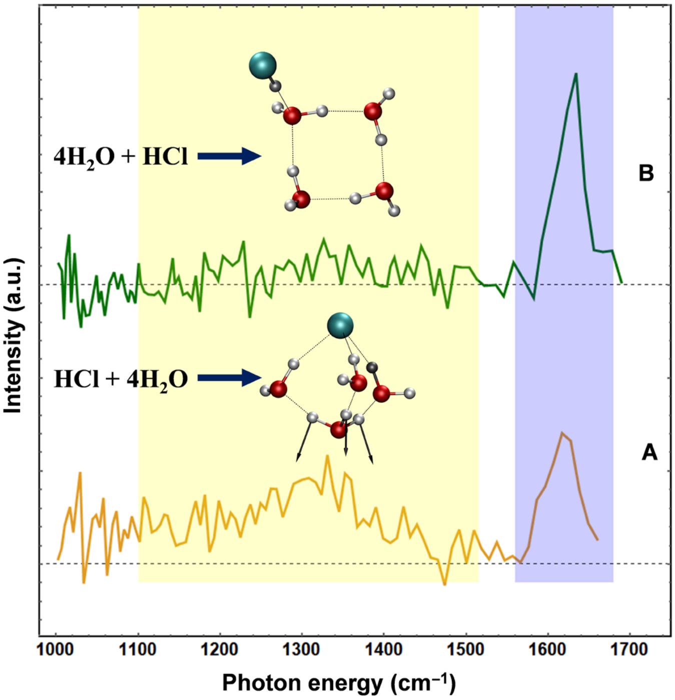

Fig. 3. Comparison of the IR spectra of mixed $HCl\text{-}H_2{}^{18}O$ clusters, measured at *m*/*z* = 41, for two distinct experimental scenarios. (**A**) HCl pickup precedes the pickup of water molecules. (**B**) Water pickup precedes the pickup of HCl.

candidates (see the "Structure search and harmonic analysis of $HCl(H_2O)_n$ species" section in the Supplementary Materials) are exclusively formed, namely, the $n = 5$ solvent-shared and contact ion pairs SIP_5 and CIP_5 depicted in fig. S8, whose H_3O^+ umbrella motion frequencies (unscaled harmonic MP2) are red-shifted by 51 and 128 cm^{-1} with reference to the $n = 4$ SIP species, respectively (see table S1). Given that anharmonicity effects and, thus, red shifts in the umbrella frequency of SIP have been shown to be small (*39*), whereas enormous anharmonicities are expected for the corresponding contact ion pair CIP (*41*, *42*), we performed ab initio path integral simulations at ultralow temperatures (see the "Nuclear quantum effects on $n = 5$ CIP versus SIP species" section in the Supplementary Materials). In stark contrast to SIP_5, in which the three O—H bonds within H_3O^+ are similar and well localized, the one pointing toward Cl^- in CIP_5 is extremely anharmonic because of pronounced anisotropic quantum delocalization (see fig. S9). This implies that the harmonic umbrella mode of CIP_5 should be enormously red-shifted. Together, these findings suggest that the broad resonance in Fig. 1D, which is red-shifted by ~32 cm^{-1}, can be assigned to the umbrella mode of species SIP_5, as depicted in the molecular model in Fig. 1D.

What happens if the pickup order of HCl and H_2O is reversed (cell 1, $H_2{}^{18}O$; cell 2, HCl) while keeping the individual pressures unchanged ($H_2{}^{18}O$, 0.53 mPa; HCl, 0.14 mPa)? As mentioned earlier, under these conditions, the formation of cyclic water tetramer,

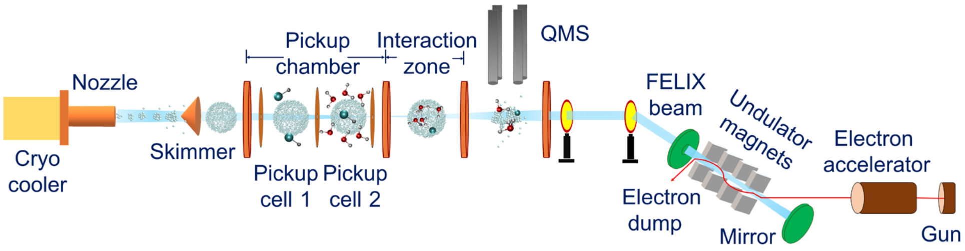

Fig. 4. Schematics of the helium droplet machine at the FELIX Laboratory (BoHeNDI@FELIX). QMS, quadrupole mass spectrometer.

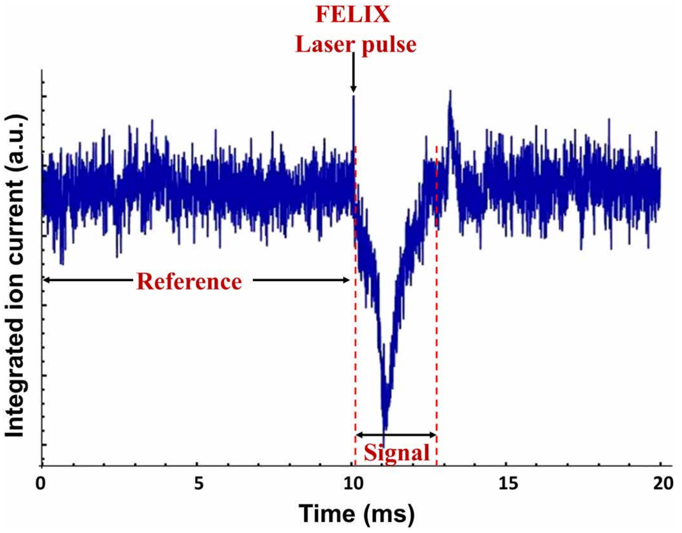

Fig. 5. $m/z = 41$ ion current, for pure $H_2{}^{18}O$ clusters, as a function of time, is shown as a representative example. The ion current was integrated over several measurements in the frequency range of 1000 to 1700 cm^{-1}. Ion current before 10 ms was used as a reference. The ion current in the ~10- to 13-ms time window contains depletion signal.

pentamer, and hexamer is expected with an estimated relative population of ~55, ~30, and ~15%, respectively. This cyclic ring formation is then followed by a subsequent aggregation process of HCl. We recorded the spectra at $m/z = 41$, with this reverse pickup order. In this case, no spectral fingerprint for hydronium (see Fig. 3B) could be detected in the expected frequency window. Given that four H_2O molecules suffice to dissociate HCl at ultralow temperatures (*9*, *10*, *36*), the absence of the hydronium band indicates either the formation of the well-known $n = 4$ ion pair (CIP), which escapes detection in the measured frequency range subject to its large red-shifted H_3O^+ umbrella fingerprint, or an absence of the H_3O^+ moiety in the formed cluster. Considering our S/N ~ 10 in the measured frequency range, even if the SIP cluster is formed, it must be less than 10% of that formed with HCl first, water second pickup order. The molecular underpinnings, revealed by ab initio aggregation simulations (see the "Ab initio aggregation simulations of cyclic $(H_2O)_4$ with HCl" section in the Supplementary Materials), unmask the underlying mechanism: Aggregating one HCl with the cyclic $(H_2O)_4$ isomer, which is the preferred water tetramer formed in helium nanodroplets (*34*), does not lead to the dissociation of HCl despite four water molecules being available. Instead, HCl either remains attached to the $(H_2O)_4$ ring by donating an H-bond forming the aggregated (AG) structure (see Fig. 3B) or inserts itself into the cyclic water tetramer via two different pathways, each leading to the known undissociated (UD) structure (see the "Ab initio aggregation simulations of cyclic $(H_2O)_4$ with HCl" section in the Supplementary Materials).

CONCLUSIONS

We showed that HCl completely dissociates on stepwise addition of four water molecules forming an SIP, $H_3O^+(H_2O)_3Cl^-$. Addition of the fifth water molecule is proposed to result in the formation of an SIP_5, $H_3O^+(H_2O)_4Cl^-$, leaving the H_3O^+ moiety intact. Moreover, our experiments supported by our state-of-the-art ab initio simulations showed that HCl dissociation is highly sensitive to the sequence in which molecular aggregation takes place. For HCl, dissociation occurs readily upon stepwise microsolvation with water molecules, whereas its interaction with preexisting cryogenic ice-like water clusters does not lead to low-barrier proton transfer from acid to water. These findings unveil that the fundamental question of whether acid dissociation and, therefore, any subsequent acid/base chemistry can take place at ultralow temperatures does not have a simple "yes" or "no" answer (see Fig. 2). Thus, "dissociation" and "no dissociation" are just two sides of the same coin. It is expected that this discovery is by no means unique to the generic HCl/water system but is a general feature of cryochemical reactions at ultracold conditions: Sequence matters!

MATERIALS AND METHODS

Experimental

Experiments were performed using a helium droplet isolation apparatus coupled with the high-power FEL at FELIX Laboratory, Nijmegen. Spectroscopy in helium droplets is a well-established technique that facilitates the studies of individual molecules or molecular aggregates as well as reactions at ultracold conditions (0.37 K) (*9*, *43*). While the pure droplets are transparent to radiation in the terahertz to ultraviolet range, molecules that are embedded in the droplets can absorb radiation. Because of weak interaction between the embedded molecule(s) and surrounding helium atoms, the matrix-induced shifts for a vibrational transition are small, usually <2 cm^{-1} for rovibrational transitions, as compared to the gas-phase spectra (*43*). The weakly interacting nature of helium atoms is also responsible for the fast evaporative cooling (10^{10} K/s) of the molecules to the ground rovibrational state, as observed in helium droplets (*43*).

Our experimental setup is shown schematically in Fig. 4, which has earlier been described in detail (*35*). The helium droplet apparatus consists of four differentially pumped vacuum chambers. In the first chamber, helium at pressures from 30 to 60 bar is precooled to temperatures between 10 and 22 K, using a Leybold Coolpower-130 closed-cycle cold head, and continuously expanded through a 5-μm-diameter nozzle, which leads to the formation of the superfluid helium droplets, with an equilibrium temperature of 0.37 K. The droplet size is log-normal distributed and can be controlled by varying the He pressure and temperature. In the work reported here, we used expansion conditions of 40 bar and 14 K, which result in an average helium droplet size of about 10,000 He atoms.

The second vacuum chamber (see Fig. 4 and fig. S1) contains two individually pumped, spatially well-separated (distance, ~20 cm) pickup cells that are traversed by the droplet beam via 5-mm-diameter openings in the cell walls. Each cell has its own sample inlet line, which was used to provide either HCl gas or water vapor as a dopant. Ultrahigh purity HCl gas (99.995% purity) was obtained from Air Liquide, and isotopically pure $H_2{}^{18}O$ (isotopic purity 97% atoms of ^{18}O) was obtained from Aldrich. These were used without further purification except for the freeze-pump-thaw degassing of water. Dopant pressures were regulated using high-precision dosing valves (model: VAT-59024-GE01) and were accurate to within 1×10^{-7} mbar. Even for high water pressures, the increase in the background pressure for the other pickup cell was small, indicating that HCl-water cross-contamination between the pickup cells was negligible.

The FELs at the FELIX Laboratory in Nijmegen, Netherlands, were used as the IR radiation source to excite the dopant molecules in an antiparallel configuration. The ultrabright FELs at FELIX cover the spectral range 80 to 3600 cm^{-1} with a frequency resolution of ~0.5% of the central frequency. The radiation of the FELs consists of a train of macropulses (5 to 8 μs) with a 10-Hz repetition rate. Each macropulse contains several thousand micropulses of picosecond time duration, separated by 1 ns. In the frequency range reported here, typical energies for micro- and macropulses amount to 20 μJ and 80 mJ, respectively. The excitation energy of the dopant molecules is rapidly dissipated via evaporation of helium atoms, which results in reduced average droplet size. The reduction in the droplet size depends linearly on the macropulse energy. After passing through a ~1-m-long spectroscopy region, the droplets were ionized via electron impact ionization and detected with a quadrupole mass spectrometer. Because the ionization cross section is proportional to the droplet size, the ionization yield is decreased when the dopant is in resonance, causing evaporation of helium (depletion spectroscopy).

For each FELIX-macropulse, ion current was recorded for a total of 20 ms, 10 ms before the arrival of the macropulse and 10 ms afterward (see Fig. 5). While the FELIX-macropulses are of the order of microsecond time duration, the radiation-induced depletion signal is present for ~3-ms duration, which corresponds to the flight time of the droplets in the machine (typical droplet velocity, ~400 m/s). For each measurement, the average ion current before the arrival of the laser pulse (0- to 10-ms time window) served as a "reference." The ion current in a time window of ~10 to 13 ms contains the depletion signal [see also (*35*)].

Theoretical

Geometry optimization

Geometry optimization calculations were performed using the BLYP functional (*44*, *45*) together with the aug-cc-pVTZ basis set and were validated by using resolution-of-identity second-order Møller–Plesset (MP2) (*46*) optimizations in conjunction with the larger basis set aug-cc-pVQZ, as provided by the TURBOMOLE package (*47*). All the structures were characterized to be minima based on harmonic vibrational frequency analysis.

In addition, single-point calculations using the BLYP and MP2 optimized structures were performed using the DLPNO-CCSD(T) method (*48*), as implemented in ORCA (*49*). The extrapolation of the energies to the complete basis set (CBS) limit was performed using the def2-TZVPP and def2-QZVPP basis sets using the default CBS implementation in ORCA (*49*).

Quantum effects

Ab initio path integral molecular dynamics simulations were performed at 1.25 K. All electrons were treated explicitly at the BLYP/aug-cc-pVTZ level, as implemented in the CP2K code (*50*). The path integral was represented using $P = 64$ beads (also known as Trotter replica), which enforces convergence of the quantum discretization in conjunction with using PIGLET thermostatting in CP2K, as developed and benchmarked recently for ultralow temperatures (*51*).

Aggregation simulations

Ab initio aggregation simulations were performed with the CPMD code (*52*) using the BLYP functional. The structures were centered in a cubic cell with a box length of 20 Å. Efficient Car-Parrinello propagation of the ab initio molecular dynamics equations of motion was used with a time step of 4 a.u. (atomic units) (corresponding to about 0.097 fs) in case of canonical ensemble (NVT) and of 5 a.u. for microcanonical ensemble (NVE) simulations together with a fictitious electron mass of 760 a.u. while using the deuterium mass for hydrogen atoms.

SUPPLEMENTARY MATERIALS

Supplementary material for this article is available at http://advances.sciencemag.org/cgi/content/full/5/6/eaav8179/DC1

Section S1. Experimental design and additional results

Section S2. Simulation methods and additional results

Fig. S1. Details of the second vacuum chamber.

Fig. S2. Variation of ion current at $m/z = 36$ with HCl partial pressure in cell 1.

Fig. S3. Dependence of the ion current upon water partial pressure as detected on $m/z = 41, 61,$ and 81.

Fig. S4. Reference ion current, as a function of $H_2{}^{18}O$ partial pressure, detected at mass channels $m/z = 41, 61,$ and 81.

Fig. S5. Variation of the spectroscopic signal (red dots) as a function of $H_2{}^{18}O$ partial pressure for different mass channels and frequencies.

Fig. S6. Poisson fit assuming a superposition of two Poisson distributions for pickup of $(H_2O)_4$ and $(H_2O)_5$.

Fig. S7. Relevant structures of the $HCl(H_2O)_4$ cluster as well as that of the Eigen complex, $(H_3O)^+(H_2O)_3$, all optimized using BLYP.

Fig. S8. Relevant structures of the $HCl(H_2O)_5$ cluster all optimized using BLYP.

Fig. S9. Quantum O—H distance distribution functions of the three protons and the oxygen within the hydronium moiety of the CIP_5 (top) and SIP_5 (bottom) conformers at 1.25 K.

Fig. S10. Mechanism leading to the formation of CIP_5 after the aggregation of the fifth water molecule with the $HCl(H_2O)_4$ SIP C_3 conformer in terms of representative snapshots sampled from the ab initio aggregation simulations.

Fig. S11. Mechanism leading to the formation of SIP_5 (right) via attachment of the fifth water molecule to the Cl site of the SIP C_1 conformer (left) in terms of representative snapshots sampled from the ab initio aggregation simulations.

Fig. S12. Mechanism leading to the formation of the cyclic UD structure (bottom left) after the aggregation of the HCl molecule with the cyclic water tetramer $(H_2O)_4$ has generated the AG structure (top left) in terms of representative snapshots sampled from the ab initio aggregation simulations.

Fig. S13. Alternative mechanism leading to the formation of the cyclic UD structure (bottom left) after the aggregation of the HCl molecule with the cyclic water tetramer $(H_2O)_4$ has generated the AG structure (top left) in terms of representative snapshots sampled from the ab initio aggregation simulations.

Table S1. Relative electronic energy (without inclusion of zero-point energy correction), dipole moment, and (unscaled harmonic) frequency of the hindered umbrella mode of the hydronium moiety, H_3O^+, in case of ion pair structures for the most relevant $HCl(H_2O)_n$ isomers with $n = 4$ and 5, based on optimized MP2 and BLYP structures.

Table S2. Aggregation simulations of SIP + H_2O with initial NVT electrostatic steering alignment of the water molecule.

Table S3. Aggregation simulations of SIP + H_2O with the water molecule in random orientations and positions around the center of the SIP cluster.

Table S4. Aggregation simulations of the cyclic $(H_2O)_4$ cluster with an HCl molecule using three different classes of initial conditions, using different cluster-molecule distances (d), relative velocities (v), and harmonic constants (k), as specified.

References (*53*, *54*)

REFERENCES AND NOTES

1. J.-C. Jiang, Y.-S. Wang, H.-C. Chang, S. H. Lin, Y. T. Lee, G. Niedner-Schatteburg, H.-C. Chang, Infrared spectra of $H^+(H_2O)_{5-8}$ clusters: Evidence for symmetric proton hydration. *J. Am. Chem. Soc.* **122**, 1398–1410 (2000).
2. J. P. Devlin, N. Uras, J. Sadlej, V. Buch, Discrete stages in the solvation and ionization of hydrogen chloride adsorbed on ice particles. *Nature* **417**, 269–271 (2002).
3. K. R. Asmis, N. L. Pivonka, G. Santambrogio, M. Brümmer, C. Kaposta, D. M. Neumark, L. Wöste, Gas-phase infrared spectrum of the protonated water dimer. *Science* **299**, 1375–1377 (2003).
4. M. Rini, B.-Z. Magnes, E. Pines, E. T. J. Nibbering, Real-time observation of bimodal proton transfer in acid-base pairs in water. *Science* **301**, 349–352 (2003).
5. J.-W. Shin, N. I. Hammer, E. G. Diken, M. A. Johnson, R. S. Walters, T. D. Jaeger, M. A. Duncan, R. A. Christie, K. D. Jordan, Infrared signature of structures associated with the $H^+(H_2O)_n$ ($n = 6$ to 27) clusters. *Science* **304**, 1137–1140 (2004).
6. M. Miyazaki, A. Fujii, T. Ebata, N. Mikami, Infrared spectroscopic evidence for protonated water clusters forming nanoscale cages. *Science* **304**, 1134–1137 (2004).
7. J. M. Headrick, E. G. Diken, R. S. Walters, N. I. Hammer, R. A. Christie, J. Cui, E. M. Myshakin, M. A. Duncan, M. A. Johnson, K. D. Jordan, Spectral signatures of hydrated proton vibrations in water clusters. *Science* **308**, 1765–1769 (2005).
8. S. Woutersen, H. J. Bakker, Ultrafast vibrational and structural dynamics of the proton in liquid water. *Phys. Rev. Lett.* **96**, 138305 (2006).
9. A. Gutberlet, G. Schwaab, Ö. Birer, M. Masia, A. Kaczmarek, H. Forbert, M. Havenith, D. Marx, Aggregation-induced dissociation of $HCl(H_2O)_4$ below 1 K: The smallest droplet of acid. *Science* **324**, 1545–1548 (2009).
10. M. Letzner, S. Gruen, D. Habig, K. Hanke, T. Endres, P. Nieto, G. Schwaab, Ł. Walewski, M. Wollenhaupt, H. Forbert, D. Marx, M. Havenith, High resolution spectroscopy of HCl-water clusters: IR bands of undissociated and dissociated clusters revisited. *J. Chem. Phys.* **139**, 154304 (2013).
11. M. H. Elkins, H. L. Williams, A. T. Shreve, D. M. Neumark, Relaxation mechanism of the hydrated electron. *Science* **342**, 1496–1499 (2013).
12. M. Thämer, L. De Marco, K. Ramasesha, A. Mandal, A. Tokmakoff, Ultrafast 2D IR spectroscopy of the excess proton in liquid water. *Science* **350**, 78–82 (2015).
13. C. T. Wolke, J. A. Fournier, L. C. Dzugan, M. R. Fagiani, T. T. Odbadrakh, H. Knorke, K. D. Jordan, A. B. McCoy, K. R. Asmis, M. A. Johnson, Spectroscopic snapshots of the proton-transfer mechanism in water. *Science* **354**, 1131–1135 (2016).
14. F. Dahms, B. P. Fingerhut, E. T. J. Nibbering, E. Pines, T. Elsaesser, Large-amplitude transfer motion of hydrated excess protons mapped by ultrafast 2D IR spectroscopy. *Science* **357**, 491–495 (2017).
15. J. O. Daldrop, M. Saita, M. Heyden, V. A. Lorenz-Fonfria, J. Heberle, R. R. Netz, Orientation of non-spherical protonated water clusters revealed by infrared absorption dichroism. *Nat. Commun.* **9**, 311 (2018).
16. D. Marx, Proton transfer 200 years after von Grotthuss: Insights from ab initio simulations. *ChemPhysChem* **8**, 209–210 (2007).
17. B. J. Gertner, J. T. Hynes, Molecular dynamics simulation of hydrochloric acid ionization at the surface of stratospheric ice. *Science* **271**, 1563–1566 (1996).
18. D. C. Clary, Molecules on ice. *Science* **271**, 1509 (1996).
19. K. Bolton, J. B. C. Pettersson, Ice-catalyzed ionization of hydrochloric acid. *J. Am. Chem. Soc.* **123**, 7360–7363 (2001).
20. M. S. Gudipati, J. Castillo-Rogez, *The Science of Solar System Ices* (Springer, 2013).
21. E. F. van Dishoeck, L. E. Kristensen, A. O. Benz, E. A. Bergin, P. Caselli, J. R. Goicoechea, J. Cernicharo, F. Herpin, M. R. Hogerheijde, D. Johnstone, R. Liseau, B. Nisini, R. Shipman, M. Tafalla, F. van der Tak, F. Wyrowski, Water in star-forming regions with the Herschel Space Observatory (WISH). I. Overview of key program and first results. *Publ. Astron. Soc. Pac.* **123**, 138–170 (2010).
22. M. Goto, J. D. Bailey, S. Hocuk, P. Caselli, G. B. Esplugues, S. Cazaux, M. Spaans, The first frost in the Pipe Nebula. *Astron. Astrophys.* **610**, A9 (2018).
23. M. R. Hogerheijde, E. A. Bergin, C. Brinch, L. I. Cleeves, J. K. J. Fogel, G. A. Blake, C. Dominik, D. C. Lis, G. Melnick, D. Neufeld, O. Panić, J. C. Pearson, L. Kristensen, U. A. Yildiz, E. F. Van Dishoeck, Detection of the water reservoir in a forming planetary system. *Science* **334**, 338–340 (2011).
24. L. I. Cleeves, E. A. Bergin, C. M. O'D. Alexander, F. Du, D. Graninger, K. I. Öberg, T. J. Harries, The ancient heritage of water ice in the solar system. *Science* **345**, 1590–1593 (2014).
25. L. Hornekær, A. Baurichter, V. V. Petrunin, D. Field, A. C. Luntz, Importance of surface morphology in interstellar H_2 formation. *Science* **302**, 1943–1946 (2003).
26. S. Solomon, R. R. Garcia, F. S. Rowland, D. J. Wuebbles, On the depletion of Antarctic ozone. *Nature* **321**, 755–758 (1986).
27. M. J. Molina, T.-L. Tso, L. T. Molina, F. C.-Y. Wang, Antarctic stratospheric chemistry of chlorine nitrate, hydrogen chloride, and ice: Release of active chlorine. *Science* **238**, 1253–1257 (1987).
28. H. Kang, T.-H. Shin, S.-C. Park, I. K. Kim, S.-J. Han, Acidity of hydrogen chloride on ice. *J. Am. Chem. Soc.* **122**, 9842–9843 (2000).
29. P. Parent, C. Laffon, Adsorption of HCl on the water ice surface studied by X-ray absorption spectroscopy. *J. Phys. Chem. B* **109**, 1547–1553 (2005).
30. M. Ončák, P. Slavíček, V. Poterya, M. Fárník, U. Buck, Emergence of charge-transfer-to-solvent band in the absorption spectra of hydrogen halides on ice nanoparticles: Spectroscopic evidence for acidic dissociation. *J. Phys. Chem. A* **112**, 5344–5353 (2008).
31. P. Parent, J. Lasne, G. Marcotte, C. Laffon, HCl adsorption on ice at low temperature: A combined X-ray absorption, photoemission and infrared study. *Phys. Chem. Chem. Phys.* **13**, 7142–7148 (2011).
32. J. P. Devlin, H. Kang, Comment on "HCl adsorption on ice at low temperature: A combined X-ray absorption, photoemission and infrared study" by P. Parent, J. Lasne, G. Marcotte and C. Laffon, *Phys. Chem. Chem. Phys.*, 2011, 13, 7142. *Phys. Chem. Chem. Phys.* **14**, 1048–1049 (2012).
33. P. Parent, J. Lasne, G. Marcotte, C. Laffon, Reply to the 'Comment on "HCl adsorption on ice at low temperature: A combined X-ray absorption, photoemission and infrared study"' by J. P. Devlin and H. Kang, *Phys. Chem. Chem. Phys.*, 2012, 14, DOI: 10.1039/c1cp22007a. *Phys. Chem. Chem. Phys.* **14**, 1050–1053 (2012).
34. K. Nauta, R. E. Miller, Formation of cyclic water hexamer in liquid helium: The smallest piece of ice. *Science* **287**, 293–295 (2000).
35. D. Mani, T. Fischer, R. Schwan, A. Dey, B. Redlich, A. F. G. Van Der Meer, G. Schwaab, M. Havenith, A helium nanodroplet setup for mid and far-infrared spectroscopy using pulsed-free-electron lasers: Vibrational spectra of propargyl alcohol. *RSC Adv.* **7**, 54318–54325 (2017).
36. H. Forbert, M. Masia, A. Kaczmarek-Kedziera, N. N. Nair, D. Marx, Aggregation-induced chemical reactions: Acid dissociation in growing water clusters. *J. Am. Chem. Soc.* **133**, 4062–4072 (2011).
37. M. Lewerenz, B. Schilling, J. P. Toennies, Successive capture and coagulation of atoms and molecules to small clusters in large liquid helium clusters. *J. Chem. Phys.* **102**, 8191–8207 (1995).
38. R. Schwan, M. Kaufmann, D. Leicht, G. Schwaab, M. Havenith, Infrared spectroscopy of the ν_2 band of the water monomer and small water clusters $(H_2O)_{n=2,3,4}$ in helium droplets. *Phys. Chem. Chem. Phys.* **18**, 24063–24069 (2016).
39. J. S. Mancini, J. M. Bowman, Isolating the spectral signature of H_3O^+ in the smallest droplet of dissociated HCl acid. *Phys. Chem. Chem. Phys.* **17**, 6222–6226 (2015).
40. S. D. Flynn, D. Skvortsov, A. M. Morrison, T. Liang, M. Y. Choi, G. E. Douberly, A. F. Vilesov, Infrared spectra of HCl-H_2O clusters in helium nanodroplets. *J. Phys. Chem. Lett.* **1**, 2233–2238 (2010).
41. Ł. Walewski, H. Forbert, D. Marx, Quantum induced bond centering in microsolvated HCl: Solvent separated versus contact ion pairs. *J. Phys. Chem. Lett.* **2**, 3069–3074 (2011).
42. Ł. Walewski, H. Forbert, D. Marx, Revealing the subtle interplay of thermal and quantum fluctuation effects on contact ion pairing in microsolvated HCl. *Chemphyschem* **14**, 817–826 (2013).
43. M. Y. Choi, G. E. Douberly, T. M. Falconer, W. K. Lewis, C. M. Lindsay, J. M. Merritt, P. L. Stiles, R. E. Miller, Infrared spectroscopy of helium nanodroplets: Novel methods for physics and chemistry. *Int. Rev. Phys. Chem.* **25**, 15–75 (2006).
44. A. D. Becke, Density-functional exchange-energy approximation with correct asymptotic behavior. *Phys. Rev. A* **38**, 3098–3100 (1988).
45. C. Lee, W. Yang, R. G. Parr, Development of the Colle-Salvetti correlation-energy formula into a functional of the electron density. *Phys. Rev. B* **37**, 785–789 (1988).
46. F. Weigend, M. Häser, RI-MP2: First derivatives and global consistency. *Theor. Chem. Acc.* **97**, 331–340 (1997).
47. Turbomole Version 6.2; http://www.turbomole.com.
48. M. Saitow, U. Becker, C. Riplinger, E. F. Valeev, F. Neese, A new near-linear scaling, efficient and accurate, open-shell domain-based local pair natural orbital coupled cluster singles and doubles theory. *J. Chem. Phys.* **146**, 164105 (2017).
49. F. Neese, Software update: The ORCA program system, version 4.0. *Wiley Interdiscip. Rev. Comput. Mol. Sci.* **8**, e1327 (2018).
50. CP2K; www.cp2k.org.
51. F. Uhl, D. Marx, M. Ceriotti, Accelerated path integral methods for atomistic simulations at ultra-low temperatures. *J. Chem. Phys.* **145**, 054101 (2016).
52. CPMD; www.cpmd.org.
53. A. Vargas-Caamal, J. L. Cabellos, F. Ortiz-Chi, H. S. Rzepa, A. Restrepo, G. Merino, How many water molecules does it take to dissociate HCl? *Chem. A Eur. J.* **22**, 2812–2818 (2016).
54. R. Pérez de Tudela, D. Marx, Acid dissociation in HCl-water clusters is temperature dependent and cannot be detected based on dipole moments. *Phys. Rev. Lett.* **119**, 223001 (2017).

Acknowledgments: We would like to thank T. Fischer and C. Can for helping in the initial installment of the setup at FELIX and J. Bowman for useful discussions. **Funding:** We gratefully acknowledge the Stichting voor Fundamenteel Onderzoek der Materie (FOM) and

Laserlab-Europe grant 654148 for the support of the FELIX Laboratory. This work was funded by the Deutsche Forschungsgemeinschaft (DFG, German Research Foundation) under Germany's Excellence Strategy – EXC-2033 – Project number 390677874. **Author contributions:** D. Mani, G.S., and M.H. conceived and designed the experiments. D. Mani, R.S., N.P., and G.S. performed the experiments. D. Mani, G.S., and M.H. analyzed and interpreted the experimental data. D. Marx and H.F. conceived the simulation approaches. R.P.d.T. and S.K. performed all computations and analyzed the computational data together with H.F. and D. Marx. B.R. and A.F.G.v.d.M. were in charge of the FELs at the FELIX Laboratory. D. Mani, R.P.d.T., G.S., D. Marx, and M.H. wrote the manuscript. **Competing interests:** The authors declare that they have no competing interests. **Data and materials availability:** All data needed to evaluate the conclusions in the paper are present in the paper and/or the Supplementary Materials. Additional data related to this paper may be requested from the authors.

Submitted 23 October 2018
Accepted 2 May 2019
Published 7 June 2019
10.1126/sciadv.aav8179

Citation: D. Mani, R. P. de Tudela, R. Schwan, N. Pal, S. Körning, H. Forbert, B. Redlich, A. F. G. van der Meer, G. Schwaab, D. Marx, M. Havenith, Acid solvation versus dissociation at "stardust conditions": Reaction sequence matters. *Sci. Adv.* **5**, eaav8179 (2019).

Science Advances

Acid solvation versus dissociation at "stardust conditions": Reaction sequence matters

Devendra Mani, Ricardo Pérez de Tudela, Raffael Schwan, Nitish Pal, Saskia Körning, Harald Forbert, Britta Redlich, A. F. G. van der Meer, Gerhard Schwaab, Dominik Marx and Martina Havenith

Sci Adv **5** (6), eaav8179.
DOI: 10.1126/sciadv.aav8179

ARTICLE TOOLS http://advances.sciencemag.org/content/5/6/eaav8179

SUPPLEMENTARY MATERIALS http://advances.sciencemag.org/content/suppl/2019/06/03/5.6.eaav8179.DC1

REFERENCES This article cites 50 articles, 16 of which you can access for free
http://advances.sciencemag.org/content/5/6/eaav8179#BIBL

PERMISSIONS http://www.sciencemag.org/help/reprints-and-permissions

Use of this article is subject to the Terms of Service

Science Advances (ISSN 2375-2548) is published by the American Association for the Advancement of Science, 1200 New York Avenue NW, Washington, DC 20005. 2017 © The Authors, some rights reserved; exclusive licensee American Association for the Advancement of Science. No claim to original U.S. Government Works. The title *Science Advances* is a registered trademark of AAAS.